Q:1, 2, 3, 4, 5, 6, 7

Energetic basis for calcium phosphate mineralization by amelogenin variants: Insights into the origin of *amelogenesis imperfecta*

Jinhui Tao[a], Yongsoon Shin[a], Rajith Jayasinha[a], Garry W. Buchko[a,b], Sarah D. Burton[a], Alice Dohnalkova[a], Zheming Wang[a], Wendy J. Shaw[a], and Barbara J. Tarasevich[a,1]

Q:8 [a]Pacific Northwest National Laboratory, Richland, WA 99354; and [b]School of Molecular Biosciences, Washington State University, Pullman, WA 99164

Edited by David Baker, University of Washington, Seattle, WA, and approved May 20, 2019 (received for review October 1, 2018)

Small variations in the primary amino acid sequence of extracellular matrix proteins can have profound effects on the biomineralization of hard tissues. For example, a change in one amino acid within the amelogenin protein can lead to drastic changes in enamel phenotype, resulting in *amelogenesis imperfecta*, enamel that is defective and easily damaged. Despite the importance of these undesirable phenotypes, there is very little understanding of how single amino acid variation in amelogenins can lead to malformed enamel. Here, we aim to develop a thermodynamic understanding of how protein variants can affect steps of the biomineralization process. High-resolution, in situ atomic force microscopy (AFM) showed that altering one amino acid within the murine amelogenin sequence (T21I, P41T, and P71T) resulted in an increase in the quantity of protein adsorbed onto hydroxyapatite (HAP) and the formation of multiple protein layers. Quantitative analysis of the equilibrium adsorbate amounts revealed that the protein variants had higher oligomer–oligomer binding energies. MMP20 enzyme degradation and HAP mineralization studies showed that the amino acid variants slowed the degradation of amelogenin by MMP20 and inhibited the growth and phase transformation of HAP. We propose that the protein variants cause malformed enamel because they bind excessively to HAP and disrupt the normal HAP growth and enzymatic degradation processes. The in situ methods applied to determine the energetics of molecular level processes are powerful tools toward understanding the mechanisms of biomineralization.

biomineralization | protein adsorption | amelogenin

The biomineralization of hard tissue structures is guided by proteins that are excreted into extracellular spaces, initiating nucleation and controlling mineral growth. Tooth enamel is an exquisite example of a biomineral that is controlled by proteins, primarily amelogenin, the dominant protein in the enamel extracellular matrix (1). In normal enamel formation, ameloblasts secrete wild-type amelogenin and other proteins into the extracellular matrix. Amorphous calcium phosphate (ACP) particles Q:10 nucleate and grow within the protein matrix to form long, thin structures that are oriented parallel to each other and are separated by protein matrix (2). The needle-like structures continue to grow lengthwise as the ameloblasts retract from the growth front. In vitro (3) and in vivo (2) studies have shown that amelogenin monomers self-assemble into quaternary structures called oligomers and nanospheres. These protein structures can bind onto hydroxyapatite (HAP) and affect the growth (4), crystallite aspect ratio (5), and spacing of the crystallites (6). Enzymes are secreted during the secretory stage (MMP20) and beginning of the maturation stage (KLK4) of amelogenesis and proteolytically degrade the extracellular matrix proteins (7). Protein degradation and removal corresponds to transformation of the amorphous needles into HAP (8), the widening of the crystals laterally, and a resulting structure that is 95% mineral. Adjacent crystals coalesce into the unusually long and highly aligned rods that contribute to making enamel one of the hardest minerals formed biologically (1).

When ameloblasts secrete amelogenins altered by one amino acid into the extracellular matrix, there are dramatic changes in the enamel phenotype resulting in enamel that is defective and easily damaged. This phenotype is called *amelogenesis imperfecta* (9, 10) and can be caused by point mutations on the AMELX gene (11, 12). The most commonly studied single amino acid variants are T21I and P41T. For example, mice containing a transgene resulting in the P41T variant of amelogenin resulted in enamel that was rough and very thin (13). There is very little known about how changing one amino acid residue in the protein can affect the HAP mineralization process so drastically. The protein variants could alter the important steps involved in normal enamel formation: amelogenin binding to growing crystals, enzymatic degradation behavior, and crystal growth and morphology. Previously, we employed high resolution, in situ atomic force microscopy (AFM) to study the energetics of amelogenin binding and the identification of adsorbed structures onto single crystal HAP (100) to elucidate how protein binding can control enamel formation (14). In this work, we aim to develop an energetic description of how single amino acid variants of amelogenin can affect steps of the biomineralization process compared with wild-type amelogenin. An understanding of how subtle changes in biomacromolecule sequence affect mineralization processes can

Significance

Protein binding is important to many biological processes such as biomineralization, cell signaling, and enzyme interactions. We found that protein binding is key in explaining how single amino acid changes in amelogenin can lead to adverse effects on the biomineralization of hydroxyapatite (HAP) in tooth enamel. A normal amount of protein adsorption resulted in HAP formation and the enzymatic removal of protein from HAP surfaces by MMP20 for the wild-type amelogenin, rpM179. Excessive protein binding, however, inhibited HAP formation and slowed the removal of protein by MMP20 for T21I, P41T, and P71T single amino acid variants. Excessive protein binding may be an important factor in explaining how single amino acid variants cause the *amelogenesis imperfecta* phenotype in vivo.

Author contributions: J.T., R.J., W.J.S., and B.J.T. designed research; J.T., Y.S., R.J., G.W.B., S.D.B., A.D., Z.W., and B.J.T. performed research; Z.W. contributed new reagents/analytic tools; J.T., Y.S., R.J., and B.J.T. analyzed data; and B.J.T. wrote the paper.

The authors declare no conflict of interest.

This article is a PNAS Direct Submission.

[1]To whom correspondence may be addressed. Email: barbara.tarasevich@pnnl.gov.

This article contains supporting information online at www.pnas.org/lookup/suppl/doi:10.1073/pnas.1815654116/-/DCSupplemental.

greatly contribute to an understanding of biomineralization and the predictive synthesis of functional materials by macromolecular design.

Results

Oligomer–HAP and Oligomer–Oligomer Interactions. The adsorption of naturally occurring single amino acid variants T21I, P41T, an experimental variant, P71T, and wild-type rpM179 (*SI Appendix*, Fig. S1) onto single crystal HAP (100) surfaces was studied by in situ AFM in real time (Fig. 1 and Movies S1–S7). Even though the variants formed ∼25- to 30-nm-diameter (100- to 200-mer) nanospheres in solution, as evidenced by dynamic light scattering (DLS) (*SI Appendix*, Fig. S2), the adsorbates onto HAP were smaller particles (5- to 6-nm height × 20-nm diameter), estimated to be ∼21- to 45-mer oligomers (*SI Appendix*, Fig. S3). Since it is well known that amelogenin nanospheres are composed of oligomeric substructures (3), we propose that the variant proteins adsorb by disassembly of the nanospheres into oligomeric subunits, similar to the adsorption mechanism we have shown previously for rpM179 and the histidine-tagged amelogenin, rp(H)M180 (14).

The kinetics of protein adsorption onto HAP at 15.6 μg/mL are shown in Fig. 2*A*, and at other protein concentrations in the *SI Appendix*, Fig. S4. The protein coverage was determined from the AFM-measured area of the oligomer (adjusted for tip diameter) relative to the entire area. The protein coverage increased with time until an equilibrium coverage was reached. At low coverage, the adsorbates consisted of isolated oligomers or small clusters of oligomers, and at high coverage, the adsorbates formed dense monolayers of oligomers (Fig. 1). An analysis of the equilibrium coverages of the various proteins over a range of solution protein concentrations was found to fit the Hill model (*SI Appendix*, Eq. **S4**), as shown in Fig. 2*C*, but not the Langmuir model. The Hill analysis describes a cooperative effect on binding quantified by the Hill coefficient, n, where protein can bind to the surface by interacting with protein already adsorbed when n is greater than 1 (15). Cooperative binding is consistent with the tendency of amelogenin oligomers to self-assemble into higher order structures.

Interestingly, more variant P41T and P71T protein bound to HAP compared with rpM179, as shown in Fig. 2*A* at 15.6 μg/mL protein concentration and in the Hill plots in Fig. 2*C*. A previous study also showed the increased adsorption of P41T onto HAP nanoparticles compared with the wild-type protein (16). Single amino acid changes in the central and N-terminal regions of amelogenin, therefore, led to increases in binding compared with the wild-type protein.

At protein concentrations <63 μg/mL, adsorption resulted in the formation of, at most, a single monolayer of oligomers at equilibrium. Increasing the protein concentration to ≥63 μg/mL, however, resulted in a striking change in adsorption behavior for all of the variants, from the initial formation of a single oligomer monolayer to the adsorption of a second protein layer, as shown in Fig. 2*B*, *SI Appendix*, Fig. S5, and Movies S5–S7. At 125 μg/mL, the first layer of oligomers was close to full coverage within

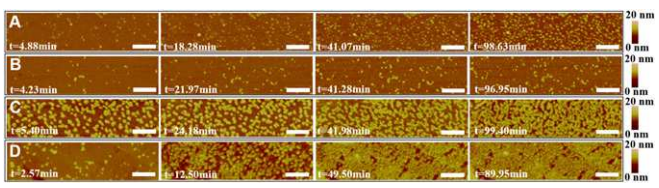

Fig. 1. In situ AFM images of the first layer of amelogenin adsorbed onto the HAP (100) face (pH 8.0) at different time points and a protein concentration of 15.6 μg/mL rpM179 (*A*), T21I (*B*), P41T (*C*), and P71T (*D*). (Scale bar, 200 nm.)

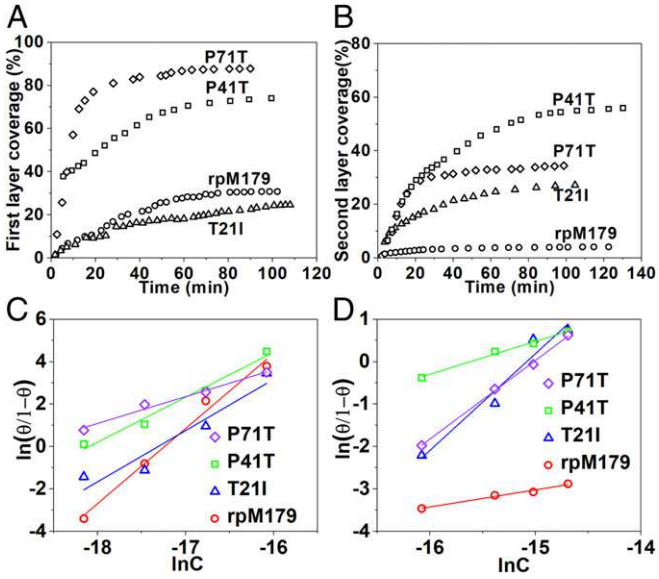

Fig. 2. Kinetics of protein adsorption at 15.6 μg/mL concentration for the first adsorbed layer (*A*) and at 125 μg/mL concentration for the second adsorbed layer (*B*). Hill plot analysis of ln (θ/1 − θ) versus ln C, where θ is the equilibrium protein coverage and C is the solution protein concentration for the first adsorbed layer (*C*) and the second adsorbed layer (*D*).

5 to 10 min, and then the second layer started to form. As many as two layers were adsorbed for the variant proteins at a concentration of 250 μg/mL In contrast, rpM179 adsorbed primarily as a single oligomer monolayer with a second layer at very low coverage for concentrations as high as 250 μg/mL The variant bilayer adsorbates were composed of oligomers with a broader size distribution compared with the first layer (*SI Appendix*, Fig. S3). Hill plots of the coverages of the second adsorbate layer as a function of protein concentration also showed significant increases in second layer adsorption for the variants compared with the wild-type protein (Fig. 2*D*). An analysis of the second adsorbed layer Hill plots in Fig. 2*D* was used to determine thermodynamic parameters for oligomer–oligomer binding, as shown in Table 1. The oligomer–oligomer binding energy was significantly higher for the variants compared with rpM179.

In addition to obtaining important overall thermodynamic information from the adsorption kinetics experiments, further studies used solid-state NMR (ssNMR) spectroscopy to obtain insights into the local structural features of the adsorbed proteins. To accomplish this, amelogenin was isotopically ^{13}C-,^{15}N-labeled specifically at the three lysine residues located near the N terminus (K24) and C terminus (K173, K175). The lysines were chosen because there are only three in the primary amino acid sequence and they are located in the C- and N-terminal regions thought to be important for protein binding to HAP and protein–protein interactions, respectively. The solid-state cross polarization (CP) dipolar-assisted rotational resonance (DARR) ^{13}C-^{13}C correlation spectra at 37 °C presented in Fig. 3 and *SI Appendix*, Fig. S6*A* show interactions between lysine backbone carbonyls (C′) and C_α, C_β, and C_γ side chain carbons for the four proteins bound to mineral. Relative to rpM179, the biggest spectral difference was for the T21I variant that showed that the C′ interaction with C_β was not observed even at lower contour levels. This indicates that the T21I variant has more mobility at the lysine residues, indicating a weaker local binding interaction of the N- and/or C terminus with HAP compared with the wild-type protein. This interpretation is supported by measurements of the relaxation values, $T_{1\rho}$, for the carbonyl resonances of the lysines, as shown in the *SI Appendix*, Fig. S6*B*. The lysine carbonyls of T21I relaxed the

Table 1. Hill coefficients (*n*) and binding energies (Δ*G*) for oligomer–HAP and oligomer–oligomer interactions on the HAP surface

Interaction	*n*	Δ*G* (k_BT)
rpM179-HAP (100)	3.54 ± 0.28	−17.2 ± 1.9
T21I-HAP (100)	2.41 ± 0.52	−17.3 ± 5.2
P41T-HAP (100)	2.12 ± 0.21	−18.1 ± 2.5
P71T-HAP (100)	1.26 ± 0.12	−18.9 ± 2.3
rpM179-rpM179	0.40 ± 0.04	−7.5 ± 1.5
T21I-T21I	2.37 ± 0.32	−15.1 ± 2.9
P41T-P41T	0.78 ± 0.05	−15.6 ± 1.4
P71T-P71T	1.85 ± 0.05	−15.0 ± 0.6

fastest, suggesting that this region was the most dynamic and the least tightly bound to the surface of HAP compared with the other variants and rpM179.

All of the proteins contained C′-C_α cross peaks centered at ∼54 ppm, a C_α chemical shift removed from the ∼56.2-ppm random-coil C_α chemical value for lysine (17). The upfield C_α perturbations suggest that all three lysine resonances are in β-sheet environments. Evidence for β-sheet structure in the C- and N-terminal region of wild-type amelogenin bound to HAP has been identified in other related ssNMR studies (18). Also, Fourier transform infrared spectroscopy-attenuated total reflectance (FTIR-ATR) studies of mineralized protein samples confirmed the presence of β-sheet structure in all of the proteins (*SI Appendix*, Fig. S7 and Table S1).

Enzymatic Degradation. An important step in enamel formation is the degradation of proteins by MMP20 secreted during the secretory stage of amelogenesis. The degradation process results in almost complete removal of protein and the growth of HAP crystals to full size (1). We studied the degradation of amelogenin adsorbed onto HAP in the presence of MMP20 using in situ AFM. Initially, we studied the degradation of the first monolayer of protein adsorbed at 32 μg/mL. The protein coverage was determined from the adsorbate areas and showed a loss of coverage upon introduction of MMP20 into the AFM solution cell for all of the proteins as shown in Fig. 4*A*. AFM images revealed that the adsorbed oligomers decreased in diameter over time, suggesting that the removal of protein initiated at the outside of the adsorbed oligomers and moved inward (*SI Appendix*, Fig. S8 and Movies S8–S11). The heights of the oligomers also decreased from the starting heights of 5 to 6 nm (*SI Appendix*, Fig. S3) to 1 to 2 nm by 2 h of degradation time (Fig. 4*B*).

Fig. 4 and Movie S8 showed that the rpM179 protein had the fastest rate of degradation, resulting in the shrinkage of the oligomers until they disappeared, leaving behind a layer of 1.5-nm-height degradation products and a few undegraded oligomers by 2 h. The loss of protein was significantly slowed for the protein variants compared with rpM179. For P41T and P71T, there was an initial linear rate of degradation followed by a slower rate of degradation at longer times. The oligomers shrank until they disappeared, but at a slower rate than rpM179, as shown in Movies S9 and S10. By 90 min of degradation time, the surface was covered with small degradation products and a moderate amount of undegraded oligomers. The remaining oligomers appeared to be clustered, suggesting that clustering slows further degradation. Although the initial rate of T21I degradation was faster than P41T and P71T, the degradation slowed at longer times, corresponding to a slowing in the shrinkage of the oligomers as shown in Movie S10. The slower shrinkage rate is reflected in the larger distribution of degradation products in Fig. 4*B* compared with the other proteins. We also performed several studies of the degradation of bilayers of variant protein adsorbed onto HAP at 180 μg/mL, as shown in the Movies S12–S15. The variant bilayer degradation rate was significantly slowed compared with the degradation of the single monolayer of rpM179.

HAP Growth and Morphology. Another important step in enamel formation is the growth of calcium phosphate crystals in the presence of amelogenin, the dominant protein in the extracellular matrix. Mineralization behavior in the presence of wild-type and variant amelogenin was monitored by changes in solution pH and showed that there was an initial period of no significant pH change (P1), a region of fast pH decrease (P2), followed by a period of slower change in pH (P3) (Fig. 5*A* and *SI Appendix*, Fig. S9). We found that stage P1 corresponded to the formation of ACP nanoparticles that were 12 to 25 nm in diameter, as shown in Fig. 5*B*. Stage P2 corresponded to the phase transformation of ACP to HAP (Fig. 5*C* and *SI Appendix*, Fig. S10), consistent with previous studies (19, 20), and stage P3 is likely to represent further phase transformation and/or classical crystal growth by ion-by-ion addition. The variant proteins had a significant effect on each step of the growth behavior at 1.0 mg/mL protein compared with the wild-type protein. The variants increased the induction time for the ACP-to-HAP transformation and reduced the total pH change between the start and end of mineralization. The induction times for P2 at 1.0 mg/mL protein increased in the order rpM179 ∼ T21I < P41T < P71T, and the pH change increased in the order P71T ∼ P41T < T21I < rpM179, as shown in the *SI Appendix*, Fig. S11. Since the pH change relates to the amount of HAP growth and the degree of ACP-to-HAP transformation, the variants inhibited the growth and phase transformation of HAP compared with rpM179.

The transmission electron microscopy (TEM) images and analyses showed that the 24-h crystallites were mostly ribbon-like HAP with relatively high aspect ratios (2.5 to 3.4), except for the controls without protein that had more plate-like crystals with aspect ratios of ∼1.85 and T21I that had aspect ratios of ∼2.0 (*SI Appendix*, Fig. S12 and Table S2). Even though T21I adsorbed more protein than rpM179 because of the bilayers, there was more growth in the width (*b* axis), resulting in more plate-like,

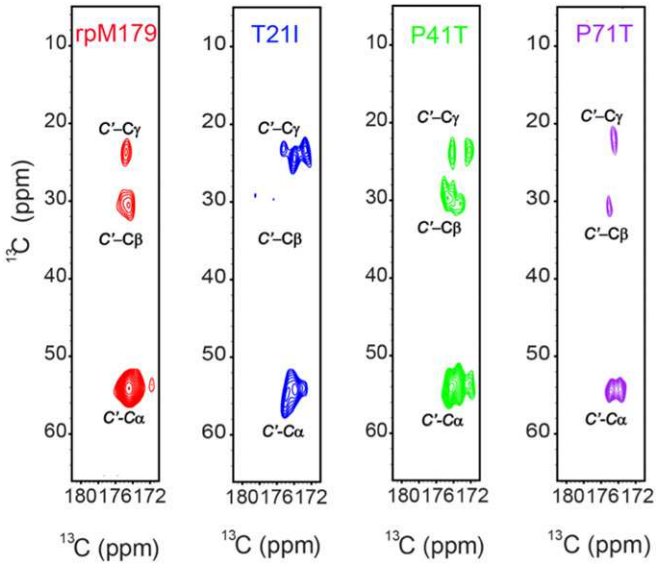

Fig. 3. Two-dimensional ^{13}C-^{13}C DARR spectra for protein mineral samples collected at a ^{1}H resonance frequency of 500 MHz (37 °C) showing the intraresidue lysine carbonyl (C′) interactions with C_γ, C_β, and C_α. Note that C′-C_β cross peaks were not observed for T21I even at lower contour levels.

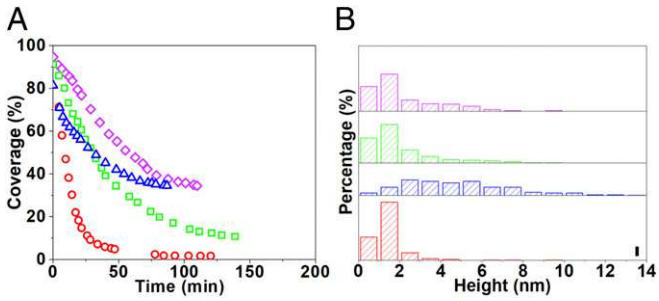

Fig. 4. The enzymatic degradation of a single monolayer of amelogenin adsorbed onto HAP (100) by MMP20, as measured by in situ AFM. (*A*) Coverages determined from the area of the adsorbates over time. (*B*) The height distribution of the adsorbates at the end of the degradation study. The height of the black scale bar represents 10%.

lower aspect ratio crystals. Less inhibition of growth in the *b* dimension may be due to the weaker local protein binding in regions around the N- and C-terminal lysines, as indicated by the ssNMR data. The weaker local interactions may allow the incorporation of calcium and phosphate to step edges and promote growth at a growth front bound by the protein. A change in mineral crystal habit as a result of subtle effects of local protein structural flexibility is striking and would be interesting to explore further.

Discussion

Excessive Protein Adsorption by Variants. Protein adsorption is believed to have an important role in the biomineralization of enamel, allowing a highly controlled growth process that places the calcium phosphate particles at regular intervals within the protein matrix, allows the calcium phosphate ribbons to be oriented parallel to each other, and limits growth until the protein is removed by proteolytic enzymes. For normal enamel formation, the wild-type amelogenin protein is completely removed by proteolytic enzymes, and the resulting HAP is dense and thick.

Our studies show that altering one amino acid within the amelogenin sequence (T21I, P41T, P71T) resulted in the excessive adsorption of oligomeric adsorbates onto HAP compared with the wild-type protein as shown schematically in Fig. 6*A*. The excessive protein adsorption occurred at low protein concentrations (<63 μg/mL) for P41T and P71T, where there was less than a monolayer of adsorbates. Although the C-terminal region has been suggested to be the main domain controlling adsorption onto HAP for wild-type protein because it is highly charged and is located on the exterior of the amelogenin oligomer (21), our results suggest that regions near T41 or T71 have important roles in promoting binding of these variants to HAP. There were no significant changes in local protein charge or hydrophobicity for variants with proline-to-threonine changes (*SI Appendix*, Fig. S13); however, it is well known that proline residues impart rigidity into a protein structure and that the removal of proline residues leads to changes in structure that increase the conformational flexibility (22). The FTIR-ATR data confirm that there are changes in secondary structure for P41T and P71T compared with rpM179. The proline-to-threonine change in P41T and P71T, therefore, leads to a more flexible structure that can become more accessible for binding to HAP (16). The changes in flexibility may promote direct interactions between regions near T41 and T71 and the HAP surface and/or may increase the exposure of the N terminus, resulting in increased binding of the N-terminal region. Fig. 6*A* shows a schematic of the proposed binding domains near T41 and T71 for monomer subunits of the adsorbed variant oligomers. The schematic picture of the adsorbed rpM179 monomer is based on literature evidence showing the C-terminal domain on the outside of the monomer (3) and the N terminus near the outside (23), yet slightly buried (24).

Excessive variant protein adsorption also occurred at higher protein concentrations (>63 μg/mL) for all of the variants, resulting in the formation of bilayers. Proline residues are commonly found in the edge strands in β-sheets and function to prevent β-sheet interactions between proteins that can lead to uncontrolled aggregation (25). The prolines at P41 and P71 may be located in edge strands of β-sheets in the N terminus that were shown in the ssNMR studies. The removal of the proline and substitution by threonine in P41T and P71T would reduce the ability of the edge strands to prevent intermolecular aggregation. This would lead to increased interactions between the β-sheet domains in the N terminus of monomers on the outside of adjacent oligomers and promote multilayer binding of oligomers onto HAP. Previous studies have shown that the aggregation of oligomers in solution was promoted for P41T at 37 °C (16). For T21I, the threonine is changed to the more hydrophobic isoleucine that could increase oligomer–oligomer binding by increasing the local hydrophobic interaction.

Effects on Enzymatic Degradation. The enzymatic removal of protein monolayer and bilayers adsorbed to HAP surfaces by MMP20 was significantly slowed for the variants, as shown schematically in Fig. 6*A*. Studies in the literature have shown that the enzymatic degradation of rpM179 by MMP20 in solution is initiated in the C-terminal region at F151 (23). A recent high-performance liquid chromatography and NMR solution study showed that MMP20 cleaved rpM179 in the C terminus at first and then in the N terminus starting at 8 h (26). The literature suggests that the enzymatic degradation in our AFM studies would be dominated by C-terminal cleavage.

It is surprising that the monolayer degradation rate slows for variant proteins that have changes at P41 and P71, when the enzymatic cleavage is in the opposite end of the protein in the C terminus. The ssNMR studies showed that there were no changes in the C-terminal structure for the variant proteins, changes that would promote variations in the C-terminal cleavage rates. Instead, we propose that the proteins have similar C-terminal enzymatic cleavage rates but different protein desorption rates. Enzymatic cleavage by MMP20 at the C-terminal site would free the C-terminal domain into the solution. Since the C-terminal region is believed to be the major binding domain for rpM179, loss of this domain would cause the rest of the

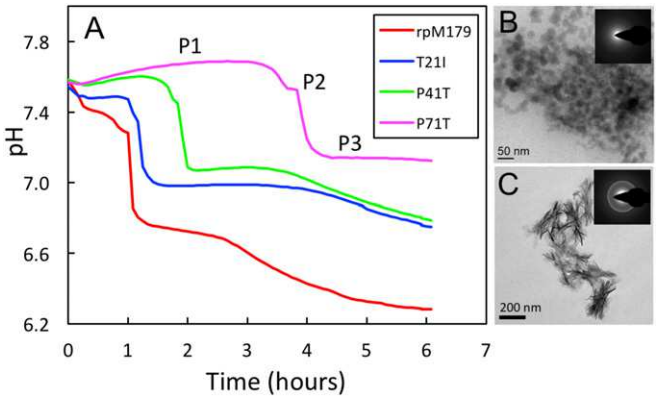

Fig. 5. (*A*) Growth kinetics of calcium phosphate in the presence of 1.0 mg/mL rpM179 (red), T21I (blue), P41T (green), and P71T (purple). The three distinct growth phases of mineral growth, P1 through P3, are labeled for P71T. TEM images from 0.2 mg/mL rpM179 solutions showing ACP nanoparticles at 30 min (*B*) and HAP crystals at 24 h (*C*). *Insets* are electron-diffraction patterns.

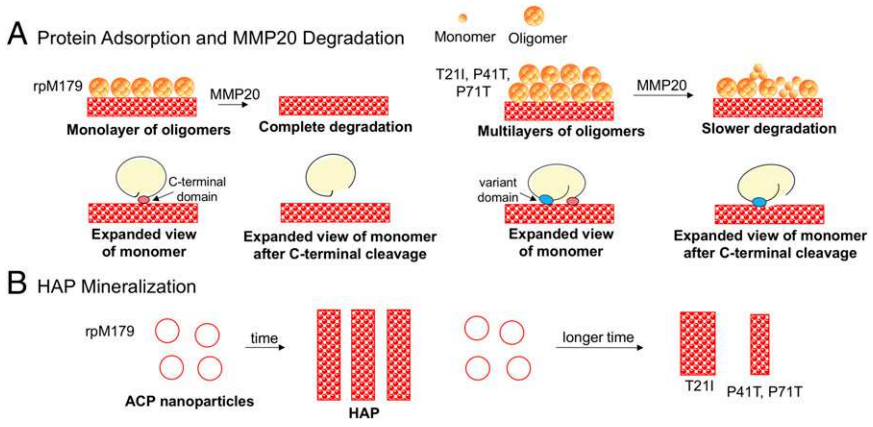

Fig. 6. (*A*) Schematic showing oligomers (composed of monomer subunits) adsorbed onto HAP under protein concentrations >63 μg/mL and the formation of oligomer monolayers for rpM179 and oligomer multilayers for the variants. The expanded view of a monomer subunit of the oligomers adsorbing onto HAP shows the C-terminal domain as the proposed primary binding domain for rpM179 and the C-terminal and the variant domain as the proposed binding domains for P41T and P71T. *A* shows how excessive binding of the amelogenin variants causes the inhibition of protein degradation by the MMP20 enzyme. The expanded view of a monomer subunit shows how desorption of the variant monomer is slowed after C-terminal cleavage compared with rpM179. *B* shows how the excessive binding of the amelogenin variants causes the inhibition of HAP formation due to longer induction times for the ACP-to-HAP transformation (longer arrow) and less HAP formation compared with rpM179 (fewer HAP crystals). The adsorbed protein involved in the ACP-to-HAP transformation is not shown for clarity.

oligomer to desorb from the surface. This is consistent with results that show that amelogenin without the C terminus adsorbs less than wild-type amelogenin (27). In contrast, the variants have significant binding interactions between the P41T and P71T regions and HAP in addition to the binding interactions between the C-terminal domain and HAP. These variants are more strongly bound to the surface because of the interactions in the N-terminal side of the protein, so they desorb more slowly once the C terminus is cleaved, as shown schematically in Fig. 6*A*. The degradation of the protein monolayer, therefore, involves cleavage in the C-terminal binding domain and protein desorption due to loss of the binding interaction with HAP.

Although the initial degradation rate of the T21I monolayers is relatively fast, the rate slows significantly over time. The loss of the hydrophilic C terminus during enzymatic cleavage combined with the isoleucine substitution may increase the hydrophobicity of the protein enough to cause binding interactions between the cleaved monomer and the oligomers. This would slow the desorption of the cleaved monomers and block further enzymatic cleavage. Also, there is some aggregation of the oligomers over time that would decrease the surface area, further reducing enzymatic cleavage rates. Degradation is further slowed for the variant bilayers formed at higher concentrations because of the higher binding amounts and stronger oligomer–oligomer interactions compared with the wild-type protein. Stronger oligomer–HAP and oligomer–oligomer binding interactions resulted in the incomplete removal of variant protein from HAP surfaces by MMP20 in our study. The excessive variant protein adsorption may lead to adverse effects on the normal enzymatic degradation process in vivo, resulting in the excess protein found in mature enamel in some cases of *amelogenesis imperfecta* (10, 12).

Effects on Mineralization. Mineralization studies revealed that HAP formation was inhibited by the amelogenin variants, especially P41T and P71T. We propose that excessive protein adsorption of the single amino acid variants slowed the growth and phase transformation of HAP, as shown schematically in Fig. 6*B*. It is well known that adsorbates can inhibit the ACP-to-HAP transformation (28), and adsorbed amelogenin has been observed to inhibit this phase transformation both in vivo (8) and in vitro (29). There are no known studies of amelogenin adsorption onto ACP, perhaps due to the instability of ACP and the difficulties in studying adsorption onto small nanoparticles. However, it would be reasonable to expect that the trends in adsorption behavior we found for the variants onto HAP would extend to variant adsorption onto the ACP nanoparticles. Variant proteins, therefore, may inhibit the ACP-to-HAP phase transformation because of stronger protein binding onto ACP.

A recent study showed that the ACP-to-HAP phase transformation involved the nucleation of HAP crystals onto the surface of ACP particles, growth of HAP and local depletion of ions, the dissolution of ACP because of the local undersaturation, and then further growth of HAP (30). The variant proteins might affect the ACP-to-HAP transformation by binding more strongly to ACP and inhibiting the nucleation of HAP. Once HAP is nucleated, variant proteins would bind more strongly to the nuclei, inhibiting HAP growth and, in turn, inhibiting ACP dissolution. Variant protein may inhibit further classical growth in phase P3 by binding to growing HAP crystallites and blocking incorporation of ions to growth sites, a mechanism well known for amelogenin and shown previously for P41T (16).

Excessive protein adsorption by the single amino acid variants resulted in the inhibition of the growth and phase transformation of HAP in our in vitro studies. Previous in vivo studies have shown that P41T and T21I variations in humans can disrupt the normal mineralization process, resulting in a form of *amelogenesis imperfecta* (11, 12) where enamel is undermineralized, porous, and soft. Excessive protein adsorption by the variants might be a factor in explaining the reduced amount of growth in this abnormal phenotype.

Although the in vivo environment is more complicated than the in vitro studies shown here, our in vitro studies point to important physicochemical phenomena that can control biomineralization in the extracellular matrix. Our studies show that altering one amino acid in amelogenin significantly retarded HAP formation and enzymatic degradation of the proteins, critical steps in the biomineralization of enamel. The small changes in sequence created large changes in adsorption behavior, and it is adsorption that modulated the mineralization and enzymatic degradation behavior, a result that has important implications for biomineralization and materials synthesis.

The in situ, high-resolution AFM methods we used are powerful tools toward understanding the mechanisms of enamel formation. They allowed us to determine oligomer–oligomer binding energies and to use the thermodynamics of adsorption processes to explain the mechanisms of abnormal biomineralization behavior. Our studies suggest that changes in local structural flexibility as a result of the proline-to-threonine variation and increases in local binding interactions in the regions near the single amino acid changes are very important and may be elucidated further by the ssNMR techniques used here. An understanding of how subtle changes in biomacromolecular structure can affect mineralization processes will greatly contribute to an understanding of biomineralization and the predictive synthesis of functional materials tailored by macromolecular design.

Experimental Section

Amelogenin Preparation and Purification. Full-length recombinant murine amelogenin, rpM179, and the protein variants of rpM179, T21I, P41T, and P71T were prepared and purified as described previously (31). Our numbering system for the variants uses the protein residue number shown in *SI Appendix*, Fig. S1 and not the revised mutation nomenclature also used in the literature that begins with the signal peptide (32). Our numbering scheme of P41T, therefore, would correspond to P70T in the revised mutation nomenclature.

Protein Solution Preparation. Solutions of rpM179, T21I, P41T, and P71T were prepared by dissolving ~5 to 10 mg/mL protein in water at pH 3 to 4. After 1 to 3 d of dissolution, the concentrations of the protein solutions were determined using UV-visible spectroscopy and the stock protein solutions were diluted into 25 mM Tris•HCl buffer adjusted to pH 8.0. These solutions were used for the dynamic light scattering (DLS) and AFM studies. The net charge and hydrophobicity of T21I, P41T, and P71T were calculated using the protein calculator at http://protcalc.sourceforge.net/ and ProtParam tool at https://web.expasy.org/protparam/,as described in *SI Appendix*.

AFM Imaging. Details of the use of AFM to study amelogenin adsorption onto micron-sized single crystals of HAP are described elsewhere (14). The adsorption kinetics of proteins at a range of solution concentrations (15.6 to 250 μg/mL) were studied at ambient temperature and were obtained from the coverage of adsorbates determined from the adsorbate areas calculated by the Particle & Pore Analysis module included in the SPIP 5.1.4 software. Equilibrium adsorption coverages for each concentration of wild-type and variant protein were obtained from at least three experiments and most of the data showed percentage errors of less than 10%. The degradation of adsorbed protein by MMP20 was studied on single monolayers of adsorbed protein adsorbed at 32 μg/mL and bilayers adsorbed at 180 μg/mL. Unadsorbed protein was flushed away with buffer, and then 400 μL of MMP20 at 4 μg/mL in Tris•HCl buffered solution was injected into the liquid cell and the in situ AFM images were collected.

NMR Mobility Studies. ssNMR samples of amelogenin mineralized with HAP were prepared using previously established protocols (3, 18). Briefly, amelogenin was prepared that was uniformly $^{13}C/^{15}N$ labeled only at the lysine residues (K24, K173, and K175). Mineralized protein samples were prepared, and the resulting crystals consisted of ribbon-like HAP with predominant (100) faces. The collected amelogenin–HAP complex was packed into a 4-mm ssNMR rotor. All 1D and 2D NMR experiments were conducted at 37 °C on a Varian VNMRS spectrometer with an 11.7 T narrow-bore magnet, operating at resonance frequencies of υ_0 (^{13}C) = 125 MHz and υ_0 (^{1}H) = 500 MHz, equipped with a triple-resonance, 4-mm, HXY Varian probe with variable temperature capability. The T1rho tau delays were adjusted from 0.005 to 12 ms. The 2D DARR studies (33) used a mixing time of 100 ms.

Mineralization Studies. Mineralization studies of calcium phosphate were performed in the presence of rpM179, T21I, P41T, and P71T. Stock solutions of protein were dissolved in water as described above and were diluted into nitrogen degassed water to give final concentrations of 0.2, 0.4, and 1.0 mg/mL protein. Aliquots of 50 mM $CaCl_2$•$2H_2O$ and 30 mM KH_2PO_4 stock solutions in water were sequentially added to give final concentrations of 2.5 mM $CaCl_2$ and 1.5 mM KH_2PO_4. The pH was increased to a final pH of 7.8 by slowly adding KOH. The sample vial was placed into a jacketed beaker at 37 °C, and the growth kinetics were monitored by changes in pH over a 6-h time period using a Microelectronics combination electrode and Orion pH meter, a method commonly used to monitor HAP formation (20). Samples were kept at 37 °C for 24 h, cooled, and the final pH at ambient temperature was recorded. Induction times for ACP-to-HAP transformation were obtained from the pH change curves. Reported induction times and ΔpH values were obtained over at least three experimental repetitions.

ACKNOWLEDGMENTS. Support for this work was provided by NIH–National Institute on Deafness and Other Communication Disorders Grant DE-015347 and the Laboratory Directed Research and Development Program at Pacific Northwest National Laboratory (PNNL) (J.T.). The research was performed at PNNL, a facility operated by Battelle for the US Department of Energy. A portion of the research was performed using the Environmental Molecular Sciences Laboratory, a national scientific user facility sponsored by the Department of Energy's Office of Biological and Environmental Research and located at PNNL.

1. A. G. Fincham, J. Moradian-Oldak, J. P. Simmer, The structural biology of the developing dental enamel matrix. *J. Struct. Biol.* **126**, 270–299 (1999).
2. A. G. Fincham *et al.*, Evidence for amelogenin "nanospheres" as functional components of secretory-stage enamel matrix. *J. Struct. Biol.* **115**, 50–59 (1995).
3. P. A. Fang, J. F. Conway, H. C. Margolis, J. P. Simmer, E. Beniash, Hierarchical self-assembly of amelogenin and the regulation of biomineralization at the nanoscale. *Proc. Natl. Acad. Sci. U.S.A.* **108**, 14097–14102 (2011).
4. E. Beniash, J. P. Simmer, H. C. Margolis, The effect of recombinant mouse amelogenins on the formation and organization of hydroxyapatite crystals in vitro. *J. Struct. Biol.* **149**, 182–190 (2005).
5. H. B. Wen, J. Moradian-Oldak, A. G. Fincham, Dose-dependent modulation of octacalcium phosphate crystal habit by amelogenins. *J. Dent. Res.* **79**, 1902–1906 (2000).
6. J. Moradian-Oldak, J. Tan, A. G. Fincham, Interaction of amelogenin with hydroxyapatite crystals: An adherence effect through amelogenin molecular self-association. *Biopolymers* **46**, 225–238 (1998).
7. J. D. Bartlett, Dental enamel development: Proteinases and their enamel matrix substrates. *ISRN Dent.* **2013**, 684607 (2013).
8. E. Beniash, R. A. Metzler, R. S. K. Lam, P. U. P. A. Gilbert, Transient amorphous calcium phosphate in forming enamel. *J. Struct. Biol.* **166**, 133–143 (2009).
9. M. J. Aldred, P. J. M. Crawford, Molecular biology of hereditary enamel defects. *Ciba Found. Symp.* **205**, 200–205, discussion 205–209 (1997).
10. D. B. Ravassipour *et al.*, Unique enamel phenotype associated with amelogenin gene (AMELX) codon 41 point mutation. *J. Dent. Res.* **79**, 1476–1481 (2000).
11. N. J. Lench, G. B. Winter, Characterisation of molecular defects in X-linked amelogenesis imperfecta (AIH1). *Hum. Mutat.* **5**, 251–259 (1995).
12. J. T. Wright *et al.*, Relationship of phenotype and genotype in X-linked amelogenesis imperfecta. *Connect. Tissue Res.* **44** (suppl. 1), 72–78 (2003).
13. C. W. Gibson *et al.*, Transgenic mice that express normal and mutated amelogenins. *J. Dent. Res.* **86**, 331–335 (2007).
14. J. Tao, G. W. Buchko, W. J. Shaw, J. J. De Yoreo, B. J. Tarasevich, Sequence-defined energetic shifts control the disassembly kinetics and microstructure of amelogenin adsorbed onto hydroxyapatite (100). *Langmuir* **31**, 10451–10460 (2015).
15. M. I. Stefan, N. Le Novère, Cooperative binding. *PLoS Comput. Biol.* **9**, e1003106 (2013).
16. L. Zhu *et al.*, Altered self-assembly and apatite binding of amelogenin induced by N-terminal proline mutation. *Arch. Oral Biol.* **56**, 331–336 (2011).
17. D. S. Wishart, B. D. Sykes, The 13C chemical-shift index: A simple method for the identification of protein secondary structure using 13C chemical-shift data. *J. Biomol. NMR* **4**, 171–180 (1994).
18. J.-X. Lu, Y. S. Xu, G. W. Buchko, W. J. Shaw, Mineral association changes the secondary structure and dynamics of murine amelogenin. *J. Dent. Res.* **92**, 1000–1004 (2013).
19. W. J. E. M. Habraken *et al.*, Ion-association complexes unite classical and non-classical theories for the biomimetic nucleation of calcium phosphate. *Nat. Commun.* **4**, 1507 (2013).
20. S. Y. Kwak *et al.*, Role of 20-kDa amelogenin (P148) phosphorylation in calcium phosphate formation in vitro. *J. Biol. Chem.* **284**, 18972–18979 (2009).
21. N. Bouropoulos, J. Moradian-Oldak, Analysis of hydroxyapatite surface coverage by amelogenin nanospheres following the Langmuir model for protein adsorption. *Calcif. Tissue Int.* **72**, 599–603 (2003).
22. D. N. Woolfson, D. H. Williams, The influence of proline residues on alpha-helical structure. *FEBS Lett.* **277**, 185–188 (1990).
23. J. Moradian-Oldak, I. Jimenez, D. Maltby, A. G. Fincham, Controlled proteolysis of amelogenins reveals exposure of both carboxy- and amino-terminal regions. *Biopolymers* **58**, 606–616 (2001).
24. J. Y. Sire, S. Delgado, D. Fromentin, M. Girondot, Amelogenin: Lessons from evolution. *Arch. Oral Biol.* **50**, 205–212 (2005).
25. J. A. Siepen, S. E. Radford, D. R. Westhead, Beta edge strands in protein structure prediction and aggregation. *Protein Sci.* **12**, 2348–2359 (2003).
26. G. W. Buchko *et al.*, Proteolytic processing of murine amelogenin and TRAP by MMP20 (Enamelysin). *Arch. Oral Biol.* (2018).
27. J. Moradian-Oldak, N. Bouropoulos, L. Wang, N. Gharakhanian, Analysis of self-assembly and apatite binding properties of amelogenin proteins lacking the hydrophilic C-terminal. *Matrix Biol.* **21**, 197–205 (2002).
28. A. S. Posner, F. Betts, N. C. Blumenthal, Role of ATP and Mg in the stabilization of biological and synthetic amorphous calcium phosphates. *Calcif. Tissue Res.* **22** (suppl.), 208–212 (1977).
29. S. Y. Kwak, Y. Yamakoshi, J. P. Simmer, H. C. Margolis, MMP20 proteolysis of native amelogenin regulates mineralization in vitro. *J. Dent. Res.* **95**, 1511–1517 (2016).
30. J. H. Tao *et al.*, Evolution of amorphous calcium phosphate to hydroxyapatite probed by gold nanoparticles. *J. Phys. Chem. C* **112**, 14929–14933 (2008).
31. G. W. Buchko, G. Lin, B. J. Tarasevich, W. J. Shaw, A solution NMR investigation into the impaired self-assembly properties of two murine amelogenins containing the point mutations T21→I or P41→T. *Arch. Biochem. Biophys.* **537**, 217–224 (2013).
32. P. S. Hart, T. C. Hart, J. P. Simmer, J. T. Wright, A nomenclature for X-linked amelogenesis imperfecta. *Arch. Oral Biol.* **47**, 255–260 (2002).
33. R. Tycko, Biomolecular solid state NMR: Advances in structural methodology and applications to peptide and protein fibrils. *Annu. Rev. Phys. Chem.* **52**, 575–606 (2001).

AUTHOR QUERIES

AUTHOR PLEASE ANSWER ALL QUERIES 1

Q: 1_Please (i) review the author affiliation and footnote symbols carefully, (ii) check the order of the author names, and (iii) check the spelling of all author names, initials, and affiliations. To confirm that the author and affiliation lines are correct, add the comment "OK" next to the author line.

Q: 2_Please review the information in the author contribution footnote carefully. Please make sure that the information is correct and that the correct author initials are listed. Note that the order of author initials matches the order of the author line per journal style. You may add contributions to the list in the footnote; however, funding should not be an author's only contribution to the work.

Q: 3_For Rajith Jayasinha, "Bridgestone" is indicated in the article metadata as the author's affiliation. Is this the author's present affiliation? If so, the following should be added as footnote "1" (and the correspondence footnote should be renumbered as "2" to match the order of the author line): (i) department/division/section/laboratory; (ii) main institution name; (iii) city and state/country location; and (iv) postal code.

Q: 4_Please note that the spelling of the following author names in the manuscript differs from the spelling provided in the article metadata: Sarah D. Burton, Alice Dohnalkova, and Zheming Wang. The spelling provided in the manuscript has been retained; please confirm.

Q: 5_Please review your open access and license selection. If any information is incorrect, please note this in the margin.

Q: 6_Per PNAS style, certain compound terms are hyphenated when used as adjectives and unhyphenated when used as nouns. This style has been applied consistently throughout where (and if) applicable.

Q: 7_Please provide a descriptive article title without the use of an em/en dash or colon (i.e., a single declarative title).

Q: 8_In the affiliations line, please provide the department/division/section as applicable for affiliation "a."

Q: 9_PNAS should be accessible to a broad scientific audience. Therefore, the nonstandard abbreviation "HAP" has been defined at its first occurrence in the Significance statement. See the sentence "We found that protein binding..."

Q: 10_Please note that nonstandard abbreviations appear at the first occurrence of their expansion and replace their expansion thereafter. Changes have been made accordingly (e.g., "ACP" has been defined here at the first occurrence of its expansion). See the sentence "Amorphous calcium phosphate (ACP) particles..."

Q: 11_Please approve the definition of the nonstandard abbreviation "TEM" here at its first occurrence (i.e., as "transmission electron microscopy"). See the sentence "The transmission electron microscopy (TEM) images..."

AUTHOR QUERIES

AUTHOR PLEASE ANSWER ALL QUERIES 2

Q: 12_Please confirm "HPLC" as spelled out here at its only occurrence (i.e., as "high-performance liquid chromatography"). Note that nonstandard abbreviations occurring only once are deleted. See the sentence "A recent high-performance liquid chromatography..."

Q: 13_PNAS does not allow claims of priority or primacy; therefore the phrase "for the first time" has been deleted in the sentence "They allowed us to determine..."

Q: 14_Please confirm the nonstandard abbreviation "UV-vis" as defined here at its only occurrence (i.e., as "UV-visible"). See the sentence "After 1 to 3 d of dissolution..."

Q: 15_Under Acknowledgments, please note that standard institutional acronyms (e.g., NIH) are not defined, whereas nonstandard institutional acronyms must be spelled out and are deleted if used only once. Please confirm the following acronyms as spelled out at their only occurrence: "NIDCH" and "EMSL" (as "National Institute on Deafness and Other Communication Disorders" and "Environmental Molecular Sciences Laboratory," respectively).

Q: 16_Please provide volume and page numbers for ref. 26.